$A1 - L1_0$ Phase Boundaries and Anisotropy via Multiple-Order-Parameter Theory for an FCC Alloy

G.B. Tanoğlu*
R.J. Braun†§
J.W. Cahn ‡
G.B. McFadden‡

Technical Report No. 2003-05

DEPARTMENT
OF
MATHEMATICAL SCIENCES

University of Delaware
Newark, Delaware

*Izmir Institute of Technology, Department of Mathematics, Gulbahcc koyu, 35437, Urla, Izmir, Turkey.

†Dept. of Mathematical Sciences, University of Delaware, Newark, DE 19716,USA.

§Author to whom correspondence should be addressed; Tel: (302)831-1869, Fax: (302) 831-4511, email: braun@math.udel.edu.

‡National Institute of Standards and Technology, Gaithersburg, MD 20899, USA

A1–$L1_0$ Phase Boundaries and Anisotropy via Multiple-Order-Parameter Theory for an FCC Alloy

G.B. Tanoğlu
Izmir Institute of Technology, Department of Mathematics
Gulbahce koyu, 35437, Urla, Izmir, Turkey

R.J. Braun*
Department of Mathematical Sciences
University of Delaware
Newark, DE 19716

J.W. Cahn and G.B. McFadden
National Institute of Standards and Technology
Gaithersburg, MD 20899
USA

January 22, 2003

Abstract

The dependence of thermodynamic properties of planar interphase boundaries (IPBs) and antiphase boundaries (APBs) in a binary alloy on an FCC lattice is studied as a function of their orientation. Using a recently-developed diffuse interface model based on three non-conserved order parameters and the concentration, and a free energy density that gives a realistic phase diagram with one disordered phase (A1) and two ordered phases ($L1_2$ and $L1_0$) such as occurs in the Cu-Au system, we are able to find IPBs and APBs between any pair of phases and domains, and for all orientations. The model includes bulk and gradient terms in a free energy functional, and assumes that there is no mismatch in the lattice parameters for the disordered and ordered phases. We catalog the appropriate boundary conditions for all IPBs and APBs. We then focus on the IPB between the disordered A1 phase and the $L1_0$ ordered phase. For this IPB we compute the numerical solution of the boundary value problem to find its interfacial energy, γ, as a function of orientation, temperature, and chemical potential (or composition). We determine the equilibrium shape for a precipitate of one phase within the other using the Cahn-Hoffman 'ξ–vector' formalism. We find that the profile of the interface is determined only by one conserved and one non-conserved order parameter, which leads to a surface energy which, as a function of orientation, is "transversely isotropic" with respect to the tetragonal axis of the $L1_0$ phase. We verify the model's consistency with the Gibbs adsorption equation.

*Author to whom correspondence should be addressed; Tel: (302) 831-1869, Fax: (302) 831-4511, email: braun@math.udel.edu

1 Introduction

In this paper we study the interphase boundaries (IPBs) and antiphase boundaries (APBs) that occur during order-disorder transitions in an fcc-based binary alloy. We employ a free energy density that provides a mean-field description of the fcc disordered phase (A1, in Strukturbericht notation) and two ordered phases, both of which have wide ranges of composition away from stoichiometry: the Cu_3Au phase, typified by the Strukturbericht $L1_2$ structure, and the CuAu(I) phase, typified by the Strukturbericht $L1_0$ structure, in the Cu–Au system. The fcc lattice can be viewed as four interpenetrating simple cubic lattices. In the disordered A1 structure, the four sublattices have equal probabilities of being occupied by either type of atom. In the $L1_2$ phase, one of the sublattices has a different occupation probability than the other three sublattices; for the $L1_0$ phase, two of the sublattices are occupied differently than the other two.

In previous work by the authors [1, 2, 3], a free energy density was employed which provided a useful description of A1–$L1_2$ IPBs and $L1_2$ APBs. In that model, however, the resulting phase diagram featured a multicritical point for all three phases [4], rather than the separate congruent disordering points with first order A1–$L1_2$ and A1–$L1_0$ transitions, as commonly observed in fcc systems such as Cu–Au. There was no co-existence of the A1 and $L1_0$ phases; the A1–$L1_0$ transition occurred only at the multicritical point and was second order. A more realistic phase diagram can be obtained with the improved free energy that we employ here; there is A1–$L1_2$ and A1–$L1_0$ coexistence and the transitions at the congruent points are both first order [5]. We are then able to obtain A1–$L1_0$ IPBs, and verify the thermodynamic consistency of the resulting model by examining, for example, the relationship due to Gibbs between changes in γ and the solute adsorption and excess entropy. We also compute the surface energy anisotropy of this IPB.

Recently, a number of continuum theories of phase change have used combinations of conserved and non-conserved order parameters with diffuse interfaces to predict or explain various phenomena in, for example, the solidification of binary alloys [6, 7, 8, 9, 10] and Ostwald ripening [11]. One method for treating diffuse interfaces is to use a free energy functional for the system based on continuum parameters that are spatially varying. The functional is written as the integral of the sum of two kinds of terms: bulk energies that are multiple-well functions of these parameters and gradient energies that are (generally quadratic) functions of the gradients of the order parameters. Both terms contribute to the energy in the transition regions that separate

bulk phases; such gradient energy models date back more than a century [12, 13].

When there is a single non-conserved scalar order parameter, the usual form of the resulting equation is the Cahn-Allen equation [14, 15]. When there is a single conserved parameter, say composition, the result is the Cahn-Hilliard equation [16, 17] used to describe the spinodal decomposition of a binary alloy. Phase-field descriptions of the solidification of binary alloys combine elements of both Cahn-Allen and Cahn-Hilliard models (e.g., [6, 7, 8, 9, 10]).

Modeling that is based on a single composition variable and one order parameter cannot fully describe the ordering in binary fcc alloys, such as Cu–Au, which have three or more different crystal structures, and many possible interfaces, such as IPBs between different structures and APBs between domains or variants of the same ordered structures. The possible crystal structures include the disordered fcc phase and two ordered phases with the prototype Cu_3Au and CuAu structures with Strukturbericht notations A1, $L1_2$ and $L1_0$, respectively. The first mean-field calculation of a phase diagram for such a system [4] gave a multiphase critical point not seen in real phase diagrams and no coexistence between A1 and $L1_0$. A more sophisticated calculation using the cluster variation method (CVM) succeeded in obtaining a realistic phase diagram [18]. This method was used for calculating APBs in $L1_2$ and the A1-$L1_2$ IPB, but it is mathematically cumbersome and was used only for some low-index orientations [19]. By using three non-conserved order parameters and by adding appropriate higher-order terms to a mean-field free energy, it became possible to obtain realistic phase diagrams [5] with a free energy functional simple enough for interface property and profile calculations at all orientations [1, 2, 3]; models in a similar vein have been developed by others [20, 21, 22, 23] and a more complete introduction is given in [2].

Single-order-parameter continuum formulations with a second order gradient energy term in cubic systems lead to isotropy of interfacial free energy γ, unless the anisotropy is introduced artificially with an orientation-dependent gradient coefficient [10, 24, 25, 26]. By anisotropy we mean how the properties of a planar interface depend on the orientation of its normal relative to the crystal axes. The multiple-order-parameter formulation leads to a natural anisotropy, i.e. without introducing ad hoc parameters in the model, in fcc [2] and even transverse to a six-fold axis in hcp [27]. Furthermore, the orientation dependence of interfacial properties (such as the interfacial energy and mobility [3]) is continuous and easily allows computation of the properties for all orientations.

In the modeling and computations by Braun *et al.* [2], the overall concentration was assumed

to be uniform across the interface; the focus was on the role played by three non-conserved order parameters in determining the anisotropy of IPBs and APBs. The model was successful in giving the anisotropy of IPBs between the disordered A1 phase and the ordered $L1_2$ phase. The wetting transition of the APB was also described. But for an IPB, a uniform composition is inconsistent with the differences in the bulk concentrations in each phase at equilibrium as given by the phase diagram. Moreover, for both APBs and IPBs, the assumption of a uniform composition leads to no adsorption, so that finding a temperature and composition-dependent interfacial free energy leads to a violation of the Gibbs adsorption equation.

We report the methods and results detailed in a recent study which examined all these interfaces in a way that was consistent with the phase equilibria obtained with the improved free energy [28]. The results are calculations of equilibrium properties, including the interfacial free energy γ, and the determination of the interface profiles which describes how the order parameter and composition vary along the normal to the interface, for all of the various types of IPBs and APBs as a function of orientation, temperature and chemical potential (or composition). In this paper, we report the general methods for studying these interfaces, which includes a catalog of APBs and IPBs, and then focus on one specific example, the IPB between the disordered fcc phase (A1) and the ordered $L1_0$ phase. We allow the concentration to vary through the interface in a manner that is consistent with the phase diagram.

In this paper we do not consider elastic energy contributions. Our model implicitly assumes that there is no mismatch in the lattice parameters for the disordered and ordered phases, so that elastic effects can be neglected. In reality, there is always a change in the lattice parameters in an order-disorder transition, though the size of the mismatch can be small; in practice, commercial alloys often have additional chemical components added to produce lattice matching. In any event, the surface properties of IPBs naturally scale differently with length than the elastic effects, with surface effects dominating at small volumes. Here we effectively restrict attention to small length scales, for which the volumetric elastic contributions to the total energy are negligible compared to the surface energy contributions. The competition between surface energy and elastic energy has been studied by a number of authors (see, e.g. [29, 30, 31]). For example, Johnson and Cahn [29] studied a bifurcation in the shape of equilibrium particles that occurs with increasing particle size. For small particles the equilibrium shape is the Wulff shape entirely determined by minimization of surface energy. Beyond a critical size, elastic energy becomes a factor in the energy minimization. To minimize total energy these larger-sized particles resemble

oblate ellipsoids, a compromise between the infinite plates that would minimize the elastic energy alone, and Wulff shapes that minimize the surface energy. In the present work we compute equilibrium shapes that resemble prolate (cigar-shaped) ellipsoids entirely from minimizing surface energy for an $L1_0$ particle embedded in A1, or vice versa, in the absence of elastic effects. Muddle, Nie, and Hugo [32] have observed equilibrium A1–$L1_0$ microstructures in Au-Cu systems with plate-like features that differ qualitatively from the equilibrium shapes that we compute. These larger-scale, plate-like structures have their origin in the theory of energy minimization in martensite transformations (see, e.g., [33]), which is beyond the scope of the present paper.

The present paper is organized as follows. The formulation is introduced in Section 2. We briefly explain the order parameters, the bulk free energy density, the bulk equilibrium states, the gradient energy contribution, and the catalog of all the interface types that can be studied with our model. The numerical method for the solution of the governing equations is presented in Section 3. In Section 4 some A1–$L1_0$ IPB results are discussed, including the verification of the Gibbs adsorption equation for an A1-$L1_0$ IPB and the transverse isotropy of the surface energy relative to the c-axis of the tetragonal $L1_0$ phase. The resulting anisotropic interface energies, their profiles, and the associated equilibrium shape for particles of one phase inside another are also given, based on Cahn-Hoffman ξ–vector formalism. Finally, a summary and discussion is given in section 5.

2 Formulation

For a binary alloy, conventional continuum theories for equilibria and kinetic processes on lattices are based on the assumption that the site occupation densities are varying slowly compared to the atomic spacing. This assumption is not valid when there is ordering; the occupation densities of adjacent sites will vary greatly if the sites belong to different ordering sublattices. Instead, by defining an occupation density ρ_j on each of the sublattices we obtain a set of quantities that are constant in each domain of an equilibrated ordered phase, and are slowly varying through the interfaces compared to the atomic spacing [34].

To describe the various ordered phases that we wish to consider for an $\mathcal{A}$–$\mathcal{B}$ binary system, we choose four sublattices as shown in Fig. 1, and denote by ρ_j the occupation density on each sublattice. Each density represents the local average atomic fraction of species $\mathcal{A}$ on that sublattice; their specification is assumed to characterize the local state of the crystal at a given temperature, $\bar{T}$.

2.1 The Order Parameters

Since the differences in the ρ_j describe the degree of order, it is convenient to introduce the parameters W, X, Y, and Z defined by

$$W = \frac{1}{4}(\rho_1 + \rho_2 + \rho_3 + \rho_4), \tag{1a}$$

$$X = \frac{1}{4}(\rho_1 + \rho_2 - \rho_3 - \rho_4), \tag{1b}$$

$$Y = \frac{1}{4}(\rho_1 - \rho_2 + \rho_3 - \rho_4), \tag{1c}$$

$$Z = \frac{1}{4}(\rho_1 - \rho_2 - \rho_3 + \rho_4). \tag{1d}$$

This definition is consistent with a local representation

$$\rho = W + X\cos(2\pi x/a) + Y\cos(2\pi y/a) + Z\cos(2\pi z/a), \tag{2}$$

where x, y, and z range over the sublattices, and a is the lattice parameter. The parameter W thus represents the overall or mean atomic fraction of the system, and the coefficients X, Y, and Z are non-conserved order parameters that can vary between $\pm 1/2$. In this model, the disordered A1 phase [35] is represented by $\rho_1 = \rho_2 = \rho_3 = \rho_4 = W$, which implies that $X = Y = Z = 0$. The ordered $L1_0$ phase is described by pairs of sublattices with equal occupation densities, which leads to a single non-zero non-conserved order parameter, $X, Y,$ or $Z \neq 0$. The ordered $L1_2$ phase is described by three sublattices whose densities are equal, and differ from the remaining sublattice density, which leads to non-conserved order parameters of equal (non-zero) magnitude, $X = \pm Y = \pm Z \neq 0$.

Scalar invariants of the order parameters are found from the symmetry of the fcc lattice [2, 23]. The first four are $(X^2 + Y^2 + Z^2)$, XYZ, $(X^4 + Y^4 + Z^4)$, and $(X^2Y^2 + Y^2Z^2 + Z^2X^2)$.

2.2 Bulk Free Energy Density

A thermodynamic description of a partially ordered crystal for the case of an isothermal system can be based on a Landau expansion of a generalized dimensionless scalar free energy density in terms of the scalar invariants [36],

$$\begin{aligned}\bar{F}(X,Y,Z,W,T) = &-\frac{\omega}{v_m}\Big[e_0(W) + e_2(W)(X^2+Y^2+Z^2) + e_3(W)XYZ + e_{41}(X^4+Y^4+Z^4) \\ &+ e_{42}(X^2Y^2 + X^2Z^2 + Y^2Z^2)\Big] + \frac{R\bar{T}}{4v_m}\sum_{i=1}^{4} I(\rho_i)\end{aligned} \tag{3}$$

where the entropy term is taken as due to ideal mixing on each sublattice,

$$I(\rho_i) = \rho_i \ln(\rho_i) + (1-\rho_i)\ln(1-\rho_i). \tag{4}$$

Here ω is the bond energy per mole, R is the universal gas constant, v_m is the molar volume; a bar denotes a dimensional variable. It is sometimes convenient to expand the entropy change on ordering in terms of these same invariants to eighth order. The ordering spinodal [37] for $L1_0$ occurs when $\partial^2 F/\partial X^2 = 0$ at $X = Y = Z = 0$. For $L1_0$ to form with a first order phase transition, it is necessary that $\partial^4 F/\partial X^4 < 0$; e_{41} has to be large and negative to overcome the positive entropy contribution.

If the internal energy E is approximated by considering only pairwise bond energies with neighbors at any distance there will be only quadratic contributions to the energy and $e_{41} = 0$. Multi-atom interactions among at least four neighbors must be considered to yield energy terms that are products of four or more ρ, which upon conversion to the X, Y, and Z parameters give contributions to e_{41}. The coefficients used for the internal energy contribution to the free energy density that give the phase diagram in Fig. 2 are given in Table 1. We will use these parameters for all computations in this paper.

2.3 Bulk States

For the free energy densities given in this section (2.3), we have nondimensionalized with $-\omega/v_m$ and the temperature has been nondimensionalized with $-\omega/R$.

If the entropy is expanded to eighth order in the order parameters it is easy to show by minimizing F with respect to the order parameters that the only minima in the free energy occur at $X = Y = Z = 0$, at $|X| = |Y| = |Z| \neq 0$ with the signs chosen to make $e_3 XYZ < 0$, and at X, Y, or $Z \neq 0$ with the other two order parameters equal to zero.

The trivial solution $X = Y = Z = 0$ represents the disordered or A1 phase. For this phase, we have from (3)

$$F_{A1}(W,T) \equiv F(0,0,0,W,T) \quad = \quad e_0(W) + T\, I(W). \tag{5}$$

For the $L1_0$ phase, corresponding to only one nonzero order parameter, the free energy is, again from (3)

$$\begin{aligned} F_{L1_0}(Z,W,T) \equiv F(0,0,Z,W,T) \quad &= \quad e_0(W) + e_2(W)Z^2 + e_{41}Z^4 + \\ &\qquad \frac{T}{2}\left[I(W+Z) + I(W-Z)\right]. \end{aligned} \tag{6}$$

Possible variants are $Z \neq X = Y = 0$, $X \neq Y = Z = 0$ or $Y \neq X = Z = 0$. This phase corresponds to alternating layers of uniform occupation densities, which is the CuAu(I) phase in the Cu–Au system [38]. Finally, for the $L1_2$ phase where $|X| = |Y| = |Z| \neq 0$, the free energy (3) becomes (with $e_3(W)Z^3 < 0$)

$$\begin{aligned} F_{L1_2}(Z,W,T) \equiv F(Z,Z,Z,W,T) &= e_0(W) + 3e_2(W)Z^2 + \\ & \quad e_3(W)Z^3 + 3(e_{41}+e_{42})Z^4 + \\ & \quad \frac{T}{4}\left[I(W+3Z) + 3I(W-Z)\right]. \end{aligned} \tag{7}$$

If $W \leq 1/2$ (see Table 1), e_3 is negative and the appropriate sign for the order parameter Z is positive. When $W \geq 1/2$, e_3 is positive and Z is negative. These two cases correspond to the two $L1_2$ phases, e.g. $CuAu_3$ and Cu_3Au.

Equilibrium phases can be found by convexification of the graphs of the three energies (5), (6), and (7) for fixed temperature. When there is a common tangent between the curves of two or three phases the points of tangency determine the compositions of the coexisting phases; the tangency points are found by solving nonlinear algebraic equations. For example, for the coexistence of A1–$L1_0$ at temperature T, we must solve

$$\frac{\partial F_{L1_0}}{\partial Z}(Z_{L1_0}, W_{L1_0}, T) = 0, \tag{8a}$$

$$\frac{\partial F_{L1_0}}{\partial W}(Z_{L1_0}, W_{L1_0}, T) = \frac{\partial F_{A1}}{\partial W}(W_{A1}, T) = \mu, \tag{8b}$$

$$F_{A1}(W_{A1}, T) - F_{L1_0}(Z_{L1_0}, W_{L1_0}, T) - \mu(W_{L1_0} - W_{A1}) = 0, \tag{8c}$$

for the unknowns Z_{L1_0}, W_{L1_0}, W_{A1} and μ where the subscripts denote the values in that phase at coexistence. Similarly, we may solve the analogous non-linear systems of equations for the $A1$–$L1_2$ and $L1_2$–$L1_0$ coexistences. These algebraic equations were all solved by using the software package DNSQ [39, 40].

Using the coefficients in Table 1 and plotting the tangent compositions as a function of temperature results in the equilibrium phase diagram of Fig. 2 (after Braun *et al.* [5]). We have chosen the coefficients so that the congruent temperature T_c at $W = W_c = 1/2$ occurs at $T = T_c \approx 2.635$. The congruent point is found from Equations (8) with $W_{A1} = W_{L1_0}$; under these conditions, both phases have identical free energy densities as well. The phase diagram is an idealized version of the Cu–Au phase diagram [38]. For example, our phase diagram is symmetrical about $W = 1/2$ and does not have the orthorhombic CuAu(II) phase

near $W = 1/2$; CuAu(II) does not appear in most other theoretical phase diagrams, such those from CVM calculations [35, 37, 41, 42].

The temperature of the congruent point for the A1–$L1_2$ transition can be normalized to a dimensional value of $\bar{T}_c = 658$K, appropriate for the Au–Cu system, by choosing the temperature scale $-\omega R/v_m = 248$K. This choice approximately fits the Au–Cu phase diagram[38], but we have made no attempt beyond this to optimize the fit of the phase diagram to other experimentally measured data. Such a fit could certainly be done.

2.4 The Gradient Energy

The symmetries associated with the A1 crystal structure restrict the possible forms of gradient energy which must be added to the free energy density. By invoking the $Fm\bar{3}m$ symmetry of the A1 crystal we find that the gradient energy term can be written in the relatively simple form [2, 23]

$$\frac{A}{2}(X_{\bar{x}}{}^2 + Y_{\bar{y}}{}^2 + Z_{\bar{z}}{}^2) + \frac{B}{2}(X_{\bar{y}}{}^2 + X_{\bar{z}}{}^2 + Y_{\bar{x}}{}^2 + Y_{\bar{z}}{}^2 + Z_{\bar{x}}{}^2 + Z_{\bar{y}}{}^2) + \frac{C}{2}|\bar{\nabla} W|^2, \tag{9}$$

where A, B and C are independent constants. The dimensional system free energy thus has the form[1]

$$\begin{aligned} \bar{\mathcal{F}} &= \int_{\bar{V}} \left\{ \bar{F}(X, Y, Z, W, T) + \frac{A}{2}(X_{\bar{x}}{}^2 + Y_{\bar{y}}{}^2 + Z_{\bar{z}}{}^2) + \frac{B}{2}(X_{\bar{y}}{}^2 + X_{\bar{z}}{}^2 + Y_{\bar{x}}{}^2 + Y_{\bar{z}}{}^2 + Z_{\bar{x}}{}^2 + Z_{\bar{y}}{}^2) \right. \\ &\quad \left. + \frac{C}{2}|\bar{\nabla} W|^2 \right\} d\bar{V}. \end{aligned} \tag{10}$$

2.5 Governing Equations for Interfaces

We wish to find equilibria which connect two coexistence phases or two domains of an equilibrium along a planar boundary. To do this we minimize the functional

$$\bar{\mathcal{I}} = \bar{\mathcal{F}} - \bar{\mu}_0 \int_{\bar{V}} W \, d\bar{V}, \tag{11}$$

with respect to the non-conserved order parameters X, Y, Z and the conserved order parameter W, with far-field boundary conditions imposed on the equilibrium phases. The second term in Equation (11) represents a constraint on the amount of solute in the volume, and the Lagrange

[1]Note the analogy with expressions for elastic energy in cubic crystals. If we let (X, Y, Z) be the analog of displacement, A is identified with C_{11}, B with C_{44}. The C_{12} term is absent because of the fcc symmetry. We emphasize, however, that the nonconserved order parameters do not constitute the components of a tensor, nor do the gradient energy coefficients transform as a fourth-rank tensor, as discussed in Appendix B of Ref. [2].

multiplier $\bar{\mu}_0$ will be seen to be the difference in the chemical potentials of the two species. When there is phase coexistence $\bar{\mu}_0 = \bar{\mu}$. Thus the governing equations are obtained as follows:

$$\frac{\delta \bar{\mathcal{I}}}{\delta X} = \frac{\delta \bar{\mathcal{I}}}{\delta Y} = \frac{\delta \bar{\mathcal{I}}}{\delta Z} = \frac{\delta \bar{\mathcal{I}}}{\delta W} = 0. \tag{12}$$

Evaluating the functional derivatives (see, e.g., [43]) gives

$$0 = AX_{\bar{x}\bar{x}} + BX_{\bar{y}\bar{y}} + BX_{\bar{z}\bar{z}} - \bar{F}_X, \tag{13a}$$

$$0 = BY_{\bar{x}\bar{x}} + AY_{\bar{y}\bar{y}} + BY_{\bar{z}\bar{z}} - \bar{F}_Y, \tag{13b}$$

$$0 = BZ_{\bar{x}\bar{x}} + BZ_{\bar{y}\bar{y}} + AZ_{\bar{z}\bar{z}} - \bar{F}_Z, \tag{13c}$$

$$0 = C(W_{\bar{x}\bar{x}} + W_{\bar{y}\bar{y}} + W_{\bar{z}\bar{z}}) - \bar{F}_W + \bar{\mu}_0. \tag{13d}$$

Here subscripts denote partial derivatives, with $X_{\bar{x}\bar{x}} = \partial^2 X/\partial \bar{x}^2$, $\bar{F}_X = \partial \bar{F}/\partial X$, etc. In this paper, we only consider stationary planar interfaces, and assume that the order parameters vary only in the direction parallel to the unit normal to the interface. We introduce a nondimensional spatial variable, distance along the normal, defined as

$$\zeta := \frac{\hat{n} \cdot \bar{\mathbf{x}}}{L_0} \tag{14}$$

where $\hat{n} = (n_x, n_y, n_z)$ denotes the unit normal, $\bar{\mathbf{x}} = (\bar{x}, \bar{y}, \bar{z})$ is the position vector and $L_0 = \sqrt{Av_m/(-\omega)}$ is the characteristic length scale. The temperature and the free energy density are made dimensionless with $-\omega/R$ and $-\omega/v_m$, respectively. This leads to the nondimensional system of ordinary differential equations

$$\lambda_x^2 X_{\zeta\zeta} = F_X(X, Y, Z, W, T), \tag{15a}$$

$$\lambda_y^2 Y_{\zeta\zeta} = F_Y(X, Y, Z, W, T), \tag{15b}$$

$$\lambda_z^2 Z_{\zeta\zeta} = F_Z(X, Y, Z, W, T), \tag{15c}$$

$$\delta^2 W_{\zeta\zeta} = F_W(X, Y, Z, W, T) - \mu_0. \tag{15d}$$

The coefficients in Equation (15) are given by

$$\lambda_x^2 = n_x^2 + \epsilon^2 n_y^2 + \epsilon^2 n_z^2, \tag{16a}$$

$$\lambda_y^2 = \epsilon^2 n_x^2 + n_y^2 + \epsilon^2 n_z^2, \tag{16b}$$

$$\lambda_z^2 = \epsilon^2 n_x^2 + \epsilon^2 n_y^2 + n_z^2. \tag{16c}$$

Here we have introduced the dimensionless parameters $\epsilon^2 = B/A$ and $\delta^2 = C/A$.

The right-hand sides in Equation (15) are nonlinear expressions which include polynomials up to fourth degree and logarithmic terms. Explicit expressions for the derivatives of F are given in Appendix A.

The equations (15) govern the transitions between bulk states for any phase boundaries allowed in the phase diagram; the bulk states provide the appropriate far-field boundary conditions for the ordinary differential equations (15) and together they constitute our model for IPBs.

2.6 Catalog and symmetries of phase boundaries

Only bulk state solutions representing the A1, $L1_2$, and $L1_0$ phases occur in the phase diagram with $W < 1/2$. In this section, we show that the symmetry of the fcc lattice and the free energy functional allows us to reduce the number of cases to three APBs and four IPBs, each for all orientations of $\hat{n}$. We note that the possibilities for APBs in this system have been enumerated by Mazauric [44], for example, but we wish to give a comprehensive list for both IPBs and APBs in the context of our model for convenience.

2.6.1 IPBs

For the A1–$L1_2$ interface the trivial solution $X = Y = Z = 0$ represents the disordered A1 phase, while $X = Y = Z \neq 0$ represents the $L1_2$ phase. Although there are 4 different variants of this phase, they are equivalent by a translation by $\frac{a}{2}\langle 110\rangle$, where a is the lattice parameter. Therefore only one possible set of boundary conditions needs to be considered for the A1–$L1_2$ interface. The symmetry of the interfacial properties as a function of $\hat{n}$, such as $\gamma(\hat{n})$ and the Wulff shape, is $m\bar{3}m$.

For the A1–$L1_0$ interface, we consider the case where $X = Y = 0$ in both the bulk regions with $Z = Z_{L1_0} \neq 0$ in the bulk $L1_0$; i.e. making z the four-fold or c-axis of $L1_0$. Since F_{L1_0} and Z_ζ^2 are even in Z, the resulting interfacial properties are identical for either sign of Z_{L1_0}. Similar symmetry arises for the other order parameters being non-zero, but the resulting energies are related by a rotation about $\langle 111\rangle$. Thus, we need only compute with a single set of boundary conditions for this case to observe the resulting interfaces and their properties. The symmetry of the interfacial properties is $4/mmm$.

For the $L1_2$–$L1_0$ interface, there are two possible boundary conditions for our system of equations. The order parameters may vary from $X = Y = Z = Z_{L1_2} > 0$ (the $L1_2$ bulk state) to $X = Y = 0$ and either to $Z = Z_{L1_0} > 0$ or to $Z = -Z_{L1_0}$ (the $L1_0$ bulk state). All other

possibilities are equivalent to one or the other of these cases. Therefore, there are two cases to be considered for $L1_2$–$L1_0$ interface. The symmetry of the interfacial properties is $4/mmm$ for both.

2.6.2 APBs

Antiphase boundaries separate two variants of the same ordered phase that necessarily share the same bulk free energy. For the $L1_2$ APB there are three possible displacement vectors that relate two variants: $\frac{a}{2}[011]$, $\frac{a}{2}[101]$, and $\frac{a}{2}[110]$. The shifts along these vectors change the sign of two of the non-conserved order parameters. Only one four-fold axis is common to both domains because the shifts move the other two of the four-fold axes of one domain to coincide with 2-fold axes of the other. The Wulff symmetry is $4/mmm$. Because of the symmetry of the free energy functional, all cases may be reduced to one possible set of boundary conditions; i.e., $X = Y = Z = Z_{L1_2} > 0$ and $-X = -Y = Z = Z_{L1_2} > 0$. All other combinations result in interfacial energies that are simply rotated and/or translated with respect to this case.

The $L1_0$ structure is formed by alternating planes of uniform occupation densities. Two possible sets of boundary conditions may be found by making changes between the two equal pairs of occupation densities. In the first set, three non-conserved order parameters may vary from $X = Y = 0$, $Z = Z_{L1_0}$ to $X = Z = 0$, $Y = Z_{10}$, a 90 degree rotation of the layers. In the second set, they may vary from $X = Y = 0$, $Z = Z_{L1_0}$ to $X = Y = 0$, $Z = -Z_{L1_0}$. All other sets can be obtained from these two sets by using appropriate rotations, so only two sets of boundary conditions need to be considered for $L1_0$ APBs.

To summarize, there are a total of seven cases to be considered for IPBs and APBs in this model of the fcc binary alloy.

3 Numerical methods

To compute solutions of the nonlinear system of ordinary differential equations (15) with the boundary conditions obtained from the phase diagram, we used two numerical methods. First, we used the boundary value problem solver COLNEW [45]; this package uses a Runge-Kutta basis on subintervals with variable spacing to provide the solution on an adaptive mesh. The solution is given as a list of coefficients for polynomials on the subintervals, but the solution may be accurately evaluated anywhere in the interval of the computation and so one is not limited to a given mesh.

In the second approach, we employed a second-order, centered finite difference approximation to the spatial derivatives and solved the resulting nonlinear algebraic equations by using DNSQ [39, 40]. For the A1–$L1_0$ IPB, we can reduce the number of differential equations in (15) to two; this makes the second method reasonably efficient. Although the second method is slower than the first, the two methods are in good agreement (up to five significant digits) when both are used.

4 Results for the A1-$L1_0$ IPB

In the previous section we saw that the seven cases considered in [28] form a catalog. Although every case can be treated with the methods developed here, we consider here just one case to illustrate the methods: the IPBs connecting the disordered A1 phase and the ordered $L1_0$ phase near the upper right hand corner of the phase diagram in Fig. 2, which could not be treated with the free energy used previously [2]. The remaining cases will be described separately [46].

For the $L1_0$ phase, $X = Y = 0$ and only Z and W are nonzero. The bulk free energy density reduces to $F_{L1_0}(Z_{L1_0}, W_{L1_0}, T)$ as given in (6). We must solve Eqn (15) subject to the boundary conditions

$$\begin{aligned} W = W_{A1},\ X = Y = Z = 0, \qquad & \text{as} \quad \zeta \quad \to \quad -\infty, \\ W = W_{L1_0},\ X = Y = 0,\ Z = Z_{L1_0}, \qquad & \text{as} \quad \zeta \quad \to \quad \infty. \end{aligned} \tag{17}$$

Numerically these conditions are applied at the ends of the computational domain, $z = \pm L$, and L is made sufficiently large that the results are insensitive to it. The equations for X and Y in (15) have the solution $X(\zeta) = Y(\zeta) = 0$, so we must solve the remaining equations for Z and W.

When we have solutions for Z and W, the interfacial energy γ may be computed from either of the followings integrals:

$$\gamma = \int_{-\infty}^{\infty} \left\{ \epsilon^2 Z_\zeta^2 + \delta^2 W_\zeta^2 \right\} d\zeta, \tag{18}$$

or

$$\gamma = \int_{-\infty}^{\infty} \left\{ \frac{\epsilon^2}{2} Z_\zeta^2 + \frac{\delta^2}{2} W_\zeta^2 + \Delta F \right\} d\zeta. \tag{19}$$

The first integral of the Euler equations and boundary conditions yield

$$\Delta F = F_{L1_0}(Z, W, T) - F_{L1_0}(0, W_{A1}, T) - (W - W_{A1}) F_{L1_0,W}(0, W_{A1}, T) = \frac{\epsilon^2}{2} Z_\zeta^2 + \frac{\delta^2}{2} W_\zeta^2. \tag{20}$$

Because of this equation the two expressions for γ, (18), and (19) are equivalent.

The solution to the system of ordinary differential equations for the planar IPB (i.e. with ζ as the only independent variable) with the given boundary conditions with $X = Y = 0$ is conjectured to give the unique minimum energy; if we have a unique minimum the appearance of additional phases in the interfacial region ("wetting behavior," see, e.g., [2]) does not occur for any orientation and temperature. Any proof that this solution to the ODE is a minimum applies only to the planar boundary and does not preclude the possibility of solutions having a microstructure with more complicated spatial dependence on x, y, and z (e.g. a zig-zag boundary) that satisfy the system of partial differential equations (13) rather than the ordinary differential equations.

4.1 Transverse Isotropy of the Surface Energy

The only dependence on the direction of the interface normal in the ordinary differential equations for Z and W is contained in λ_z^2. By expressing the components of the unit normal vector in spherical coordinates,

$$n_x = \sin\phi\cos\theta \quad n_y = \sin\phi\sin\theta \quad \text{and } n_z = \cos\phi, \tag{21}$$

where ϕ is the polar angle and θ is the azimuthal angle, from Equation (16) we find

$$\lambda_z^2 = \epsilon^2\sin^2\phi + \cos^2\phi = 1 + (\epsilon^2 - 1)\sin^2\phi, \tag{22}$$

which depends only on the polar angle, ϕ. A function of the orientation that is independent of θ, the azimuthal angle is called "transversely isotropic." We predict that γ for the A1- $L1_0$ IPB should be transversely isotropic with respect to the c-axis of the tetragonal $L1_0$ phase.

Moreover, this equation relates ϕ and ϵ to a single computational variable, λ_z. Properties are not determined by ϕ and ϵ, but by the value of λ_z according to Eqn. (22). Computing interface properties for a range of λ_z can be accomplished in a variety of ways. We have chosen to present interface profiles at $\phi = 0$, i.e., for the [001] orientation with $\lambda_z^2 = 1$, and at $\phi = 90°$, i.e., for the [100] orientation with $\lambda_z^2 = \epsilon^2$. Because of the transverse isotropy, we can use [100] to designate $\langle hk0\rangle$ results, as well as $\langle h'0l'\rangle$ to designate $\langle hkl\rangle$ results, with $h'/l' = \sqrt{h^2+k^2}/l$. The orientation dependence of interfacial energy is computed for given values of ϵ^2.

4.2 The Gibbs Adsorption Equation

We next verify that the appropriate form of the Gibbs adsorption equation holds for our model. This equation relates the variation, $d\gamma/dT$, of the surface energy of the IPB along the coexistence

region of the phase diagram to the adsorption of solute and entropy at the interface (see, e.g., [47]). Following the development given by Cahn in Ref. [48], in Appendix B we show that this equation takes the form

$$\frac{d\gamma}{dT} = -\int_{-\infty}^{\infty} \left\{ (S - S_{A1}) - (W - W_{A1}) \frac{(S_{L1_0} - S_{A1})}{(W_{L1_0} - W_{A1})} \right\} d\zeta, \tag{23}$$

where $S = -\partial F/\partial T$ is the entropy density and S_{A1} is its value in the bulk A1 phase, etc. We have computed the quantity $d\gamma/dT$ along the coexistence region and found that it agrees with our computed results for $\gamma(T)$ that were computed directly from the IPB profiles; results are given in Table 2. The first column is the temperature; column 2 is the result of evaluating (23) using the composite trapezoidal rule with computed data for the order parameters. Column 3 is a centered finite difference approximation to the numerical data plotted in Figure 9 for [001]. Columns 4 and 5 give analogous results for [100]. Good agreement is seen between the slope of the $\gamma(T)$ plot from both sources, verifying explicitly that our model and numerical solutions are consistent with the Gibbs adsorption equation.

The sign of $d\gamma/dT$ changes at orientations between [001] and [100]. Figure 3 shows $d\gamma/dT$ as a function of the azimuthal angle ϕ; the zero of $d\gamma/dT$ occurs at about 65°.

4.3 Interface profile

We next consider the interface profile and surface energy anisotropy at the congruent temperature, $T_c \approx 2.635$, and composition $W = 1/2$, for representative orientations with $\epsilon^2 = 0.005$. Figures 4 and 5 show the interface profile for the [100] and [001] orientations, respectively, at the critical temperature. From Equation (22) and the text after it, we can see that the [001] interface profile is independent of ϵ^2. Also, the [100] orientation has a sharper interface than the [001] orientation for decreasing $\epsilon^2 < 1$. The phase diagram shown in Fig. (2) is symmetric about $W = 1/2$; therefore W has the same value through the interfacial region and bulk states.

We next consider the case $T = 2.5$ for [100] and [001] orientations. The interface profiles for these orientations are in Figs. 6 and 7. Z is wider than W for [001] in Fig. 7. It is again observed that the thickness of the interface for [100] is smaller than that of the interface for [001].

4.4 Surface energy anisotropy

Since $\gamma(\phi, \theta) = \gamma(\phi)$ we can represent γ as a two-dimensional polar plot as shown in Fig. 8. As can be seen in this figure, the minimum energy occurs in the [100] direction and the maximum energy occurs in the [001] direction.

In Fig. 9 we compare the surface energies for [001] and [100] orientations as a function of temperature. The difference between the maximum and minimum energy becomes larger as the critical temperature T_c is approached; i.e., the degree of anisotropy reaches a maximum value at T_c. Strong tetragonal anisotropy is found for the range of temperatures given in Fig. 10 for $\epsilon^2 = 0.05$. In CVM computation of interfacial properties for bcc [49] and fcc [19] materials, that the difference between the interfacial energies increases at lower temperatures and then decreases at high temperatures. While it is common for materials to have the anisotropy decrease with increasing (high) temperature, it does not happen to be so for our model as we discuss shortly.

This trend of increasing anisotropy with temperature is amplified as ϵ decreases from unity. Numerical approximations of the interfacial energies at various orientations, for temperatures $T = T_c$ and $T = 2.5$ and for $\epsilon^2 = 0.005$, are compared in Table 3. By comparing Fig. 10 and Table 3, we observe that the level of anisotropy is increasing for smaller gradient energy coefficients ($\epsilon^2 = 0.005$).

In fact, the level of anisotropy increases dramatically as $\epsilon \to 0$ at the congruent point $(W, T) = (1/2, T_c)$ because $\gamma_{100} \propto \epsilon$ there. This can be seen as follows. At the congruent point, the IPB profile satisfies $W = 1/2$ and

$$\lambda_z^2 Z_{\zeta\zeta} = F_z(0, 0, Z, 1/2, T_c), \tag{24}$$

where λ_z is given in Equation (16). The interfacial energy $\gamma(n_x, n_y, n_z)$ computed from equation (24) then satisfies

$$\frac{\gamma(n_x, n_y, n_z)}{\gamma_{001}} = \sqrt{\epsilon^2(n_x^2 + n_y^2) + n_z^2}, \tag{25}$$

[c.f. Equation (6.1) in [2] for the analogous APB result]. The ratio $\gamma_{001}/\gamma_{100} = \epsilon^{-1}$ therefore diverges in the limit as $\epsilon \to 0$ at the congruent point. When $\epsilon = 1$, the IPBs are isotropic. In the model we must therefore see an increase in anisotropy as the congruent point is approached for small ϵ, since the level of anisotropy away from the congruent point remains bounded due to the contribution from the variation of the concentration W through the interface. We note that the limit $\epsilon \to 0$ corresponds to neglecting the second-nearest-neighbor interactions in the derivation of the gradient energy terms given in [2]; the remaining contributions from the nearest-neighbor terms are highly orientation-dependent.

4.5 Equilibrium Shapes

We next use the Cahn–Hoffman ξ–vector formalism [50, 51] to determine the equilibrium shapes given by the anisotropy of the interfacial energy. The ξ–vector is defined by

$$\vec{\xi} = \gamma\vec{r} + \gamma_\phi\vec{\phi} + \frac{\gamma_\theta}{\sin\phi}\vec{\theta} = \nabla[r\gamma(\phi,\theta)] \tag{26}$$

where the radial unit vector $\vec{r}(\theta,\phi) = \vec{n}$ is normal to the interface. The unit vectors $\vec{\theta}$ and $\vec{\phi}$ are tangent to the interface. The ξ–vector reduces to the form $\vec{\xi} = \gamma\vec{n}$ for the isotropic case (constant γ). In the anisotropic case, the ξ–vector is in the direction of the normal to the $1/\gamma(\theta,\phi)$ plot defined by $r = 1/\gamma(\theta,\phi)$. Its component in the radial direction is γ. To obtain the equilibrium shape, the "tail" of the ξ–vector is translated to the origin for each orientation; the collection of all the $\vec{\xi}$-vectors is then the $\vec{\xi}$-surface. The $\vec{\xi}$–surface minimizes the surface energy for a fixed volume if it is a convex shape; in that case it is identical to the Wulff shape [52, 53]. In other cases, the $\vec{\xi}$–surface is not convex and intersects itself, exhibiting "ears" (see, e.g., [2]). If the ears are excluded from the $\vec{\xi}$–surface, the remaining surface represents the equilibrium Wulff shape.

In order to compute the $\vec{\xi}$–surface for A1–L1$_0$ IPBs, γ is first obtained in terms of ϕ numerically on a regularly spaced mesh with $\Delta\phi = 1.5°$; our solutions are independent of θ. By using the formulas given in the appendix of [54], we compute $\vec{\xi}$–surface data in Cartesian coordinates. For those explicit formulas, we employ centered finite difference formulas using the discrete data in order to approximate γ_ϕ.

A cross section of the equilibrium shape for the transversely isotropic A1–L1$_0$ IPBs ($\epsilon \neq 0$) is shown in Fig. 11. The equilibrium shape is a body of revolution about [001]; the cross section perpendicular to that axis is thus a circle. The long side regions include the low-energy orientations at and near $\langle hk0\rangle$; [001] and nearby orientations have high energy and contribute little to the area of the equilibrium shape. A consequence of the increase in the level of anisotropy as $\epsilon \to 0$ is that the equilibrium shapes are increasingly elongated; they do not appear to develop missing orientations for any finite value of ϵ, however.

5 Summary and Discussion

We present a model for the free energy of a binary alloy which incorporates a model phase diagram and can be used to compute properties of diffuse-interfaces; the model uses one conserved order parameter (the composition), and three non-conserved order parameters [5]. The model can describe a variety of phase diagrams; a series of diagrams topologically similar to the Au-Cu

system was presented in [5]. It can be used for other ordered crystal structures that occur in fcc and other systems [27], though more order parameters may be required. This method allows the computation of interfaces for all orientations at a wide variety of conditions. Other methods, notably CVM, can approximate quite complicated phase diagrams, but are difficult to implement except for interfaces with low-index directions. The method is a powerful tool for computing interfaces and their motion in microstructure evolution with a natural way of incorporating anisotropy [3], and using using realistic phase diagrams.

For a phase diagram containing the A1 phase and the ordered $L1_0$ and $L1_2$ phases, similar to what is seen in the Au-Cu system, we present a catalog of the interfaces. There are IPBs that can coexist between the disordered A1 phase and the ordered $L1_0$ and $L1_2$ phases, and between the two ordered phases. The symmetry of the underlying lattice can be used to deduce that only one variant of each ordered phase is necessary to compute the anisotropy of the interfacial energy for the order-disorder IPBs; all other cases are related by simple rotation to these cases. The order-order IPBs require that the two variants of the $L1_0$ phase be used with a single $L1_2$ variant in order to compute the possible interfacial energy anisotropies; all other cases can be found by simple rotations of these two results. There are also APBs in the single phase regions of the ordered phases. For the $L1_2$ phase, only one case must be computed; for the $L1_0$ phase, two cases must be computed. Our model can compute all seven of these cases using a single formulation spanning the whole phase diagram.

The free energy density employed in this work and in Ref. [28] allows a generalization of previous work on A1 and $L1_2$ in which the composition was held fixed at the stoichiometric value for the $L1_2$ phase throughout the interface [1, 2, 3]. That free energy also prevented the consideration of the A1-$L1_0$ IPB due to the absence of coexistence between the A1 and $L1_0$ phases [4]. The new free energy allows us to focus on the interface profile and anisotropy for A1–$L1_0$ IPBs; equilibrium shapes are also computed by considering only the interfacial energy (elastic effects and lattice mismatch are neglected).

Mathematically, the problem for planar A1–$L1_0$ IPBs is a nonlinear boundary value problem which has a solution that connects two different states in the dependent variables (a heteroclinic connection). ¿From our numerically-computed solutions, we observe the profile of the interfaces, as well as compute interfacial energies. Once the energies are known, we compute equilibrium shapes using the ξ-vector.

Although we find that the IPBs energies are transversely isotropic, we also found strong

anisotropy with variations in the polar angle ϕ. The ϕ orientation dependence only served to widen or narrow the interfaces and no wetting behavior by other phases was observed. The computed compositions always varied smoothly and monotonically between the value for the A1 phase, low in this half of the phase diagram, to the higher value in the $L1_0$ phase. At the A1–$L1_0$ congruent point the composition was constant throughout the IPB; this necessarily occurred due to the symmetry of our chosen free energy and resulting phase diagram; it is not expected in a real system. Anisotropy of interfaces has also been studied using the CVM (for example [19, 44]); to our knowledge, the CVM has not been used to study the A1–$L1_0$ interface.

The transversely isotropic surface energy that we have found highlights an unexpected difficulty in using symmetry arguments to predict the surface energy anisotropy of diffuse interfaces from the high symmetry of the gradient energy. Orientation dependent surface energies in crystalline systems, and the associated Wulff shapes, reflect the symmetries of the crystals, but they are not tensor properties. Gradient energy coefficients can sometimes be shown to transform like tensors, and then the orientation dependence of γ can be deduced from the symmetry properties of such tensors. Tensors of rank 2 are transversely isotropic to 3, 4, and 6 fold axes, and thus isotropic for cubic symmetry [55]. Tensors of rank 4 are transversely isotropic to 3 and 6 fold axes. Tensors of rank 4 for a cubic system are described by three numbers and are anisotropic, unless there is a special relationship among these numbers. With an energy that is quadratic in the gradient of a single dependent variable, the gradient energy coefficient is a tensor of rank 2. We showed that the coefficients of an energy quadratic in the gradients of the three dependent variables, X, Y and Z, do not behave as tensors. Nonetheless for the fcc system we found them to be described by two of the three non-zero elements that appear in a tensor of rank four with cubic symmetry. This is consistent with what we found for the A1-$L1_2$ IPB; the Wulff shape has a marked anisotropy consistent with the cubic symmetry. But we now have found two surprises: firstly, transverse isotropy in γ and in the Wulff shape for the A1-$L1_0$ IPB with only tetragonal symmetry is greater symmetry than expected. Secondly, we found less symmetry in the hcp investigation; there was no isotropy transverse to the 6 fold axis. Here the gradient energy coefficient bore no resemblance to elements in a tensor of rank 4, which not only confirms that these coefficients are not tensors, but forms a strong counterexample to any conjecture that the orientation dependence of γ of a diffuse interface might reflect that of a low rank tensor. Both the fcc and the hcp systems each feature three nonconserved order parameters X_j and a conserved

order parameter W and the free energy functional for each model has the general form

$$\mathcal{F} = \int \left\{ c_{ijkl} X_{i,j} X_{k,l} + c_0 |\nabla W|^2 + f(X_1, X_2, X_3, W, T) \right\}. \tag{27}$$

The three nonconserved order parameters X_j and the gradient energy coefficients c_{ijkl} do not transform as tensors under changes of coordinates. For the hcp crystal, the disordered state where either type of atom is equally likely to occur on any of the four sublattices, the structure is designated A3 in Strukturbericht notation. When one of the sublattices is occupied (on average) by a different atom than the other three, the crystal structure is denoted DO_{19}; this ordered state is exactly analogous to the $L1_2$ structure on an fcc lattice.

If one were to reason by analogy with the elastic case, then, both the transverse isotropy of the A1–$L1_0$ IPB surface energy and the 6-fold anisotropy of the A3–DO_{19} IPB surface energy is unexpected. We also note that the A1–$L1_0$ IPB involves a single non-zero non-conserved order parameter, whereas the A1–$L1_2$ and A3–DO_{19} IPB involve three non-zero non-conserved order parameters. In addition, wetting by a third phase also occurs for the latter two cases, which plays a role in the observed transverse anisotropy for these IPBs. If the three non-conserved order parameters are *constrained* to remain equal throughout the interfacial region (which precludes wetting), the resulting system is effectively a single-order-parameter model, and an isotropic surface energy results.

The A1–$L1_0$ equilibrium shapes resulting from ξ–vector calculations are bodies of revolution, and no missing orientations occurred for the parameters we studied. The cross section of the anisotropic equilibrium shape (in the absence of elastic effects) is roughly an ellipse for fixed azimuthal angle θ and exactly a circle for fixed polar angle ϕ relative to the c-axis of the tetragonal $L1_0$ ([001] for the case we considered). This is in contrast to the cuboidal, nearly spherical equilibrium Wulff shapes found in our previous work for A1–$L1_2$ IPBs [1, 2] on an fcc lattice; that γ had six equal minima in the cube directions. Another contrast may be found with A3–DO_{19} IPBs in an hcp binary alloy [27]; in that situation, there is six-fold anisotropy in the plane orthogonal to the hexagonal axis. Nearly spherical equilibrium shapes are found as well but with six minima in γ distributed evenly around the equator. A concentration variable must be added to the hcp model of [27] and a phase diagram generated, in order to consider the analogous cases studied in this paper.

The variable composition added the capability to satisfy the Gibbs adsorption equation. We have verified that our model now satisfies the Gibbs adsorption equation and provides an instance

of the diffuse interface generalization of sharp interface results, as discussed in [48]. We have also verified that the numerical results obtained from the computed IPBs are in agreement with this identity.

A variation in the width of the interface with orientation is noticeable, but it does not show a dramatic widening as in cases when wetting of the phase boundary occurs (e.g., as in the A1-$L1_2$ case [2, 28]). However, in the case when the ϵ is very small and one is at the congruent point, then one must be able to resolve very thin $\langle hk0 \rangle$ interfaces (compared to [001]). In such a computation with finite difference or finite element discretizations, an adaptive mesh approach should be effective. For fixed mesh approaches, the mesh (or for a spectral method, the number of modes) must be able to resolve the thinnest interfaces.

6 Acknowledgments

GBM would like to thank the National Aeronautics and Space Administration Microgravity Research Program for support. RJB would like to thank the NSF for support via grants DMS-9722854 and DMS-9631287. GBT would like to thank the Turkish Ministry of Education for support. The authors are grateful for helpful discussions with A.A. Wheeler.

References

[1] Braun, R.J., Cahn, J.W., Hagedorn, J., McFadden, G.B. & Wheeler, A.A. Anisotropic interfaces and ordering in fcc alloys: A multiple-order-parameter continuum theory. In: Chen, L.-Q., *et al.* (eds), *Mathematics of Microstructure Evolution.* TMS/SIAM, Philadelphia, PA (1996) pp. 225–244.

[2] Braun, R.J., Cahn, J.W., McFadden, G.B. & Wheeler, A.A. Anisotropy of interfaces in an ordered alloy: a multiple-order-parameter model. *Trans. Roy. Soc. London A* **355**, (1997) 1787–1833.

[3] Braun, R.J., Cahn, J.W., McFadden, G.B., Rushmeier, H.E. & Wheeler, A.A. Theory of anisotropic growth rates in the ordering of an F.C.C. alloy. *Acta mater.* **46**, (1997) 1–12.

[4] Nix, F.C. & Shockley, W. Order-disorder transformations in alloys. *Rev. Mod. Phys.* **10**, (1938) 1–71.

[5] Braun, R.J., Zhang, J., Cahn, J.W., McFadden, G.B., & Wheeler, A.A. Model phase diagrams for an fcc alloy. In: Smith, M.K., Miksis, M.J., McFadden, G.B., Neitzel, G.P., & Canright, D.R. (eds) Proceedings of *Interfaces for the Twenty-First Century*, Imperial College Press, London (2002), pp. 213-230.

[6] Wheeler, A.A., Boettinger, W.J., and McFadden, G.B. A phase-field model for isothermal phase transitions in binary alloys, *Phys. Rev. A* **45**, (1992) 7424-7439.

[7] Caginalp, G. & Xie, W. Phase-field and and sharp-interface alloy models. *Phys. Rev. E* **48**, (1993) 1897–1909.

[8] Wheeler, A.A., Boettinger, W.J., and McFadden, G.B. A phase-field model of solute trapping during solidification, *Phys. Rev. E* **47**, (1993) 1893-1909.

[9] Ahmad, A., Wheeler, A.A., Boettinger, W.J. & McFadden, G.B. Solute trapping and solute drag in a phase-field model of rapid solidification. *Phys. Rev. E* **58**, (1998) 3436–3450.

[10] Boettinger, W.J., & Warren, J.A. Simulation of the Cell to Plane Front Transition During Directional Solidification at High Velocity *J. Crystal Growth* **200**, (1999) 583.

[11] Danan, F., Chen, L.-Q., Chen, S.P., & Voorhees, P.W. Phase field formulations for modeling the Ostwald ripening in two phase systems. *Comp. Materials Sci.* **9**, (1998) 329–336.

[12] Rayleigh, Lord On the theory of surface forces. II. Compressible fluids. *Phil. Mag.* **33**, (1892) 209–220.

[13] Waals, J.D. van der *Verhandel. Konink. Akad. Weten. Amsterdam (Sect. 1)*, 1893 **1**. (English translation, see Rowlinson, J.S. *J. Stat. Phys.* **20**, (1979) 197–244.)

[14] Cahn, J.W., & Allen, S.M. A microscopic theory for domain wall motion and its experimental verification in Fe-Al alloy domain growth kinetics. *J. Phys. (Paris) Colloque*, (1977) C7 51-54.

[15] Allen, S.M., & Cahn, J.W. A microscopic theory for antiphase boundary motion and its application to antiphase domain coarsening. *Acta metall. mater.* **27**, (1979) 1085–1095.

[16] Cahn, J.W. On spinodal decomposition. *Acta metall.* **9**, (1961) 795–801.

[17] Hilliard, J.E. Spinodal decomposition. In: Aaronson, H.I. (ed), *Phase Transformations.* American Society of Metals, Metals Park, OH (1970).

[18] Kikuchi, R., Sanchez, J.M., de Fontaine, D. & Yamauchi, H. Theoretical calculation of the Cu-Ag-Au coherent phase diagram. *Acta Metall.* **28**, (1980) 651–662.

[19] Kikuchi, R. & Cahn, J. W. Theory of interphase and antiphase boundaries in FCC alloys. *Acta Metall.* **27**, (1979) 1337–1353.

[20] Khachaturyan, A.G. *Theory of Structural Transformations in Solids*, Wiley, New York, 1983.

[21] Fan, D., & Chen, L.Q. Microstructural evolution and grain growth kinetics in a two-phase solid with quadrijunctions. In: Chen, L.-Q., *et al.*, (eds), *Mathematics of Microstructure Evolution*, TMS/SIAM, Philadelphia, PA (1996) p. 215–223.

[22] Finel, A. Thermodynamical properties of antiphases in FCC ordered alloys. In: Yavari, A., (ed), *Ordering and Disordering in Alloys*, Elsevier Applied Science, New York, NY (1992) p. 182.

[23] Lai, Z.-W. Theory of ordering dynamics for Cu_3Au. *Phys. Rev. B* **41**, (1990) 9239–9256.

[24] Kobayashi, R. Modeling and numerical simulations of dendritic crystal growth. *Physica D* **63**, (1993) 410–423.

[25] McFadden, G.B., Wheeler, A.A., Braun, R.J., Coriell, S.R., & Sekerka, R.F. Phase-field models for anisotropic interfaces. *Phys. Rev. E* **48**, (1993) 2016–2024.

[26] Taylor, J.E. & Cahn, J. W. Diffuse interfaces with sharp corners and facets: Phase field modeling of strongly anisotropic surfaces. *Physica D* **112**, (1998) 381–411.

[27] Cahn, J.W., Han, S.C., & McFadden, G.B. Anisotropy of interfaces in an ordered HCP binary alloy. *J. Stat. Phys.* **95**, (1999) 1337–1360.

[28] Tanoğlu, G.B. Phase boundaries and anisotropy via multiple-order-parameter theory for an fcc alloy. Ph.D. University of Delaware, USA. 2000.

[29] Johnson, W.C. & Cahn, J.W. Elastically induced shape bifurcations of inclusions. *Acta Mater.* **32**, (1984) 1925–1933.

[30] Johnson, W.C. & Voorhees, P.W. Elastic interaction and stability of misfitting cuboidal inhomogeneities. *J. Appl. Phys.* **61**, (1987) 1610–1619.

[31] Johnson, W.C. & Voorhees, P.W. Elastically-induced precipitate shape transitions in coherent solids. *Solid State Phenom.* **23**, (1992) 87–104.

[32] Muddle, B.C., Nie, J.F., & Hugo, G.R. Application of the theory of martensite crystallography to displacive phase transformations in substitutional nonferrous alloys. *Metal. and Mat. Trans. A*, 1994, **25**, 1841–1856.

[33] James, R.D, and Hane, K.F. Martensitic transformations and shape-memory materials. *Acta Mater.* **48**, (2000) 197–222.

[34] Novick-Cohen, A., and Cahn, J.W. Evolution equations for phase separation and ordering in binary alloys. *J. Stat. Phys.* **76**, (1994) 877–909.

[35] Ducastelle, F. *Order and Phase Stability in Alloys*, North-Holland, New York, NY (1991).

[36] Lifshitz, E.M., and Pitaevskii, L.P. *Statistical Physics, Part 1 (3rd edition)*, Pergamon, Oxford, (1980) pp. 459–471.

[37] Fontaine, D. de Cluster approach to order-disorder transformations in alloys. *Solid State Phys.* **47**, (1994) 33–176.

[38] Okamoto, H., Chakrabarti, D.J., Laughlin, D.E., & Massalski, T.B. The Au-Cu (Gold-Copper) System. *Bull. Alloy Phase Diagrams* **8**, (1987) 454–474.

[39] *SLATEC Common Math Library*, National Energy Software Center, Argonne National Laboratory, Argonne, IL. The program SNSQ was written by K.L. Hiebert and is based on an algorithm of M.J.D. Powell.

[40] Powell, M.J.D. A hybrid method for nonlinear equations. In: Rabinowitz, P. (ed), *Numerical Methods for Nonlinear Algebraic Equations*, Gordon and Breach, NJ (1988) pp. 87–161.

[41] Kikuchi, R., Fontaine, D. de Theoretical Calculations of Phase Diagrams Using the Cluster Variation Method. In: Carter, C.G. (ed), *Application of Phase Diagrams in Metallurgy and Ceramics*, NBS Special Publication 496, (1978) pp. 967–998.

[42] Kikuchi, R. Solution of the controversy in the fcc-based phase diagram. *Prog. Theo. Phys. Supp.* **87**, (1986) 69–76.

[43] Weinstock, R. *Calculus of Variations*, Dover Publications, New York, NY (1972).

[44] Mazauric, V.G. Phase diagram of domain walls in the cubic superstructures of the fcc lattice. *J. Comput.-Aided Mater. Des.* **4**, (1997) 113–132.

[45] Asher, U., Christiansen, J. & Russell, R.D. Collocation software for boundary-value ODEs. *ACM TOMS* **7**, (1981) 209–222.

[46] Tanoğlu, G.B., & Braun, R.J. A1–$L1_2$ phase boundaries and anisotropy via multiple-order-parameter theory for an fcc alloy. In preparation.

[47] McFadden, G.B. and Wheeler, A.A. On the Gibbs adsorption equation for diffuse interface models. *Proc. Roy. Soc. (London) A Mat.* 458 (2002) 1129–1149.

[48] Cahn, J.W. Thermodynamics of solid and fluid interfaces. In: *Interfacial Segregation*, ASM, Metals Park, OH (1977) pp. 3–23.

[49] Cahn, J.W. & Kikuchi, R. Theory of domain walls in ordered structures–III. Effect of substitutional deviations from stoichiometry. *J. Phys. Chem. Solids* **27**, (1966) 1305–1317.

[50] Hoffman, D.W. & Cahn, J.W. A vector thermodynamics for anisotropic surfaces. I. Fundamentals and application to plane surface junctions. *Surface Science* **31**, (1972) 368–388.

[51] Cahn, J.W. & Hoffman, D.W. A vector thermodynamics for anisotropic surfaces. II. Curved and faceted surfaces. *Acta Metall.* **22**, (1977) 1205–1214.

[52] Johnson, C.A. & Chakerian, G.D. On the proof and uniqueness of Wulff's construction of the shape of minimum surface free energy. *J. Math. Phys.* **6**, (1965) 1403-1404.

[53] Mullins, W.W. Proof that the two-dimensional shape of minimum surface free energy is convex. *J. Math. Phys.*, **3**, (1962) 754–759.

[54] Voorhees, P.W., Coriell, S.R., McFadden, G.B., and Sekerka, R.F. The effect of anisotropic crystal-melt surface tension on grain boundary groove morphology. *J. Crystal Growth* **67**, (1984) 425–440.

[55] Nye, J.F., *Physical Properties of Crystals*, Oxford University Press, Oxford (1957).

A APPENDIX A

The non-dimensional form of the Helmholtz free energy is given in the following

$$\begin{aligned} F(X,Y,Z,W,T) &= e_0(W) + e_2(W)(X^2+Y^2+Z^2) + e_3(W)XYZ + \\ & \quad e_{41}(X^4+Y^4+Z^4) + e_{42}(X^2Y^2+X^2Z^2+Y^2Z^2) + \frac{T}{4}\sum_{j=1}^{4} I(\rho_j), \end{aligned} \tag{28}$$

where $I(x)$ is given in Equation 4.

The right sides of the equations (15) are given as follows.

$$\begin{aligned} F_Z(X,Y,Z,W,T) &= 2e_2Z + e_3XY + 4e_{41}Z^3 + 2e_{42}Z(X^2+Y^2) + \\ & \quad \frac{T}{4}\ln\left[Q(X,Y,Z,W)\right], \end{aligned} \tag{29}$$

$$\begin{aligned} F_W(X,Y,Z,W,T) &= e_{0,W} + e_{2,W}(X^2+Y^2+Z^2) + e_{3,W}XYZ + \\ & \quad \frac{T}{4}\ln\left[R(X,Y,Z,W)\right]. \end{aligned} \tag{30}$$

Q and R are defined as follows:

$$\begin{aligned} Q(X,Y,Z,W) &= \frac{(W+X+Y+Z)(W-X-Y+Z)}{(1-W-X-Y-Z)(1-W+X+Y-Z)} \times \\ & \quad \frac{(1-W-X+Y+Z)(1-W+X-Y+Z)}{(W+X-Y-Z)(W-X+Y-Z)}, \end{aligned} \tag{31}$$

and

$$\begin{aligned} R(X,Y,Z,W) &= \frac{(W+X+Y+Z)(W+X-Y-Z)}{(1-W-X-Y-Z)(1-W-X+Y+Z)} \times \\ & \quad \frac{(W-X+Y-Z)(W-X-Y+Z)}{(1-W+X-Y+Z)(1-W+X+Y-Z)}. \end{aligned} \tag{32}$$

These expressions are used with $X = Y = 0$ in this paper and with $Z = 0$ where appropriate.

B APPENDIX B

Here we provide a short derivation of the Gibbs adsorption equation for our model of the A1-L1$_0$ IPB with a non-zero order parameter $Z = Z(\zeta)$, overall composition $W = W(\zeta)$, and free energy density $F_{L1_0}(Z,W,T)$; a fuller discussion in the context of general diffuse interface theories is given in Ref. [47].

For the free energy functional

$$\mathcal{F} = \int_{\infty}^{\infty} \left\{ \frac{\epsilon^2}{2} Z_\zeta^2 + \frac{\delta^2}{2} W_\zeta^2 + F_{L1_0}(Z, W, T) \right\} d\zeta, \tag{33}$$

the Euler equations, $\delta\mathcal{F}/\delta W = \mu$ and $\delta\mathcal{F}/\delta Z = 0$, yield

$$F_{L1_0,W}(Z, W, T) = \delta W_{\zeta\zeta} + \mu, \tag{34}$$

$$F_{L1_0,Z}(Z, W, T) = \epsilon^2 Z_{\zeta\zeta}, \tag{35}$$

and admit a first integral given by

$$\frac{\epsilon^2}{2} Z_\zeta^2 + \frac{\delta^2}{2} W_\zeta^2 = F_{L1_0}(Z, W, T) - F_{L1_0}(0, W_{A1}, T) - (W - W_{A1})\mu \equiv \Delta F. \tag{36}$$

Here

$$W \to W_{A1},\ Z \to 0,\ \text{as } \zeta \to -\infty, \tag{37}$$

and

$$W \to W_{L1_0},\ Z \to Z_{L1_0},\ \text{as } \zeta \to \infty, \tag{38}$$

give the far-field values of W and Z.

Evaluating the Euler equations and first integral in the far fields gives the common tangent conditions (8) that relate W_{A1}, W_{L1_0}, Z_{L1_0}, and T,

$$\mu = F_{L1_0,W}(0, W_{A1}, T) = F_{L1_0,W}(Z_{L1_0}, W_{L1_0}, T) = \frac{[F_{L1_0}(Z_{L1_0}, W_{L1_0}, T) - F_{L1_0}(0, W_{A1}, T)]}{(W_{L1_0} - W_{A1})}. \tag{39}$$

The common tangent conditions, and the equation $F_{L1_0,Z}(Z_{L1_0}, W_{L1_0}, T) = 0$, provide three relations between the four parameters W_{A1}, W_{L1_0}, Z_{L1_0}, and T, consistent with the single degree of freedom for coexistence of the bulk phases along the phase diagram. We choose to regard the temperature as the degree of freedom, and write $W_{A1} = W_{A1}(T)$ and $W_{L1_0} = W_{L1_0}(T)$.

The surface energy is given by

$$\gamma = \int_{-\infty}^{\infty} \left\{ \frac{\epsilon^2}{2} Z_\zeta^2 + \frac{\delta^2}{2} W_\zeta^2 + \Delta F \right\} d\zeta. \tag{40}$$

Since the solution can be considered to be a function of the prescribed temperature T, with $W = W(\zeta; T)$ and $Z = Z(\zeta; T)$, the surface energy of the IPB is a function of T as well. We then have

$$\frac{d\gamma}{dT} = \int_{-\infty}^{\infty} \left\{ \epsilon^2 Z_\zeta Z_{\zeta T} + \delta^2 W_\zeta W_{\zeta T} + \frac{d\Delta F}{dT} \right\} d\zeta, \tag{41}$$

which can be integrated by parts to obtain

$$\frac{d\gamma}{dT} = \int_{-\infty}^{\infty} \left\{ -\epsilon^2 Z_{\zeta\zeta} Z_T - \delta^2 W_{\zeta\zeta} W_T + \frac{d\Delta F}{dT} \right\} d\zeta. \tag{42}$$

We have

$$\frac{d\Delta F}{dT} = F_{L1_0,W}(Z,W,T)W_T + F_{L1_0,Z}(Z,W,T)Z_T + F_{L1_0,T}(Z,W,T)$$
$$-F_{L1_0,W}(0,W_{A1},T)\frac{dW_{A1}}{dT} - F_{L1_0,T}(0,W_{A1},T) - F_{L1_0,W}(0,W_{A1},T)W_T + F_{L1_0,W}(0,W_{A1},T)\frac{dW_{A1}}{dT} \tag{43}$$
$$-(W-W_{A1})F_{L1_0,WW}(0,W_{A1},T)\frac{dW_{A1}}{dT} - (W-W_{A1})F_{L1_0,WT}(0,W_{A1},T).$$

The bulk chemical potential is given by

$$\mu(T) = F_{L1_0,W}(0,W_{A1}(T),T), \tag{44}$$

and its temperature derivative is

$$\frac{d\mu}{dT} = F_{L1_0,WW}(0,W_{A1},T)\frac{dW_{A1}}{dT} + F_{L1_0,WT}(0,W_{A1},T). \tag{45}$$

The entropy is $S = -F_{L1_0,T}(Z,W,T)$, with

$$S_{A1} = -F_{L1_0,T}(0,W_{A1},T) \text{ and } S_{L1_0} = -F_{L1_0,T}(Z_{L1_0},W_{L1_0},T). \tag{46}$$

Using these definitions, the expression for $d\Delta F/dT$ simplifies to give

$$\frac{d\Delta F}{dT} = [F_{L1_0,W}(Z,W,T) - F_{L1_0,W}(0,W_{A1},T)]W_T + F_{L1_0,Z}(Z,W,T)Z_T$$
$$-[S-S_{A1}] - (W-W_{A1})\frac{d\mu}{dT}. \tag{47}$$

Inserting this expression into Eq. (42) gives

$$\frac{d\gamma}{dT} = \int_{-\infty}^{\infty} \Big\{ [F_{L1_0,Z}(Z,W,T) - \epsilon^2 Z_{\zeta\zeta}]Z_T + [F_{L1_0,W}(Z,W,T) - F_{L1_0,W}(0,W_{A1},T) - \delta W_{\zeta\zeta}]W_T$$
$$-[S-S_{A1}] - (W-W_{A1})\frac{d\mu}{dT} \Big\} d\zeta. \tag{48}$$

The first two terms vanish by virtue of the Euler equations, leading to

$$\frac{d\gamma}{dT} = -\int_{-\infty}^{\infty} \left\{ [S-S_{A1}] + (W-W_{A1})\frac{d\mu}{dT} \right\} d\zeta. \tag{49}$$

Here we note that $d\mu/dT$ is independent of ζ. It is easily seen that

$$(W_{L1_0} - W_{A1})\frac{d\mu}{dT} = -(S_{L1_0} - S_{A1}), \tag{50}$$

which can be used to provide the alternate form

$$\frac{d\gamma}{dT} = -\int_{-\infty}^{\infty} \left\{ (S-S_{A1}) - (W-W_{A1})\frac{(S_{L1_0} - S_{A1})}{(W_{L1_0} - W_{A1})} \right\} d\zeta. \tag{51}$$

e_0	$6U^2$
e_2	$-4+U^2$
e_3	$200U(1-2U^2)$
e_{41}	-12
e_{42}	15

Table 1: Coefficients used for the internal energy contribution to the free energy density (after [5]); here $U = W - 1/2$.

	[001]		[100]	
T	Eqn (23)	$d\gamma/dT$	Eqn (23)	$d\gamma/dT$
2.50	0.03174	0.03191	-0.01660	-0.01605
2.55	0.03139	0.03139	-0.01756	-0.01755
2.60	0.03099	0.03082	-0.01870	-0.01919
2.62	0.03064	0.03059	-0.01972	-0.01989
2.63	0.03045	0.03047	-0.02015	-0.02024

Table 2: Comparison of $d\gamma/dT$ for A1–L1$_0$ IPB for several temperatures for $\epsilon^2 = 0.05$, $\delta^2 = 1.0$. For columns labeled "Eqn (23)," the composite trapezoidal rule was used to evaluate the integrals with numerically computed interface profiles. The columns labeled "$d\gamma/dT$" used a centered finite difference approximation to the curve in the (T, γ) plane. The results agree to within the error of the numerical methods used.

	γ	
orientation	$T = T_c$	$T = 2.5$
[001]	0.09559	0.09193
[101]	0.06776	0.06563
[111]	0.05546	0.05435
[100]	0.00676	0.01485

Table 3: Comparison of interfacial energy for A1–L1$_0$ IPB at $T = T_c$ and $T = 2.5$ for $\epsilon^2 = 0.005$, $\delta^2 = 1.0$.

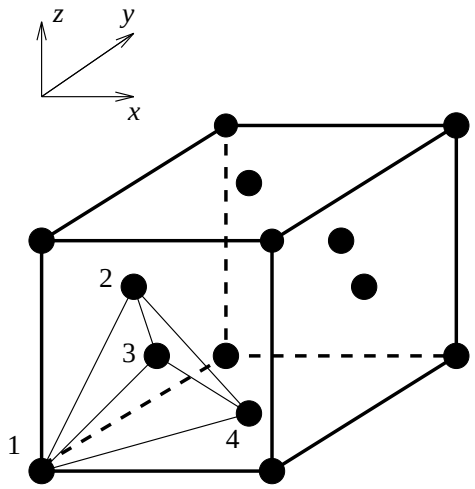

Figure 1: A schematic diagram of an fcc lattice. There are four equivalent interpenetrating simple cubic sublattices. One sublattice corresponds to the corner of the conventional unit cell, and each of the other three corresponds to the center of a face intersecting at that corner.

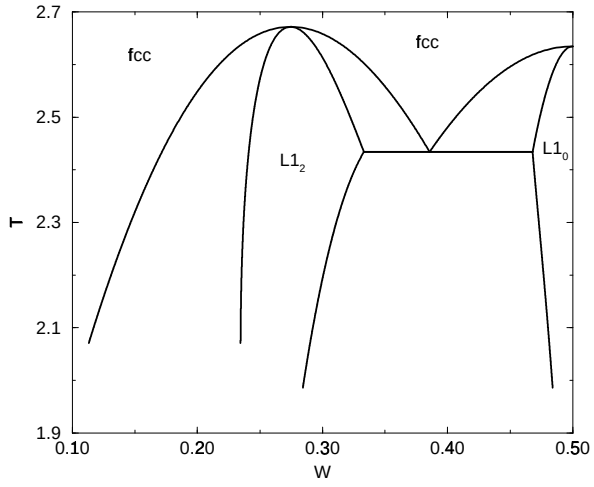

Figure 2: A model phase diagram based on the Cu–Au system, from the parameters in Table 1; note that it is symmetric about $W = 1/2$. Here fcc denotes the disordered A1 phase.

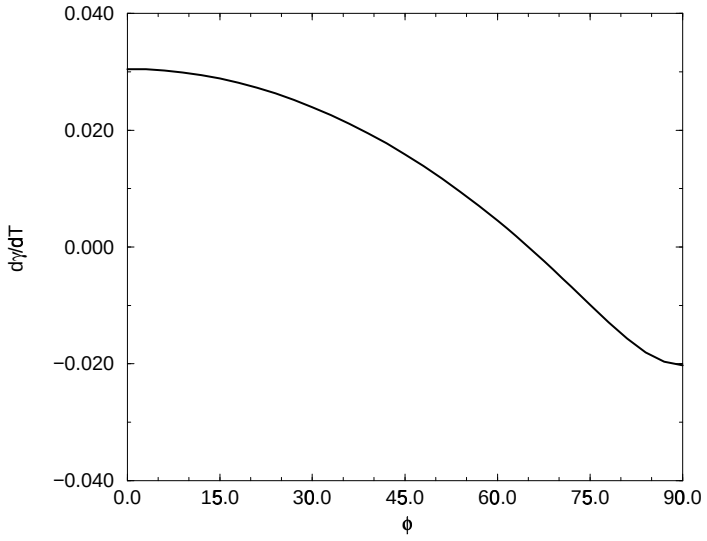

Figure 3: $d\gamma/dT$ as a function of the azimuthal angle ϕ at $T = 2.63$ for $\epsilon^2 = 0.05$ and $\delta^2 = 1.0$.

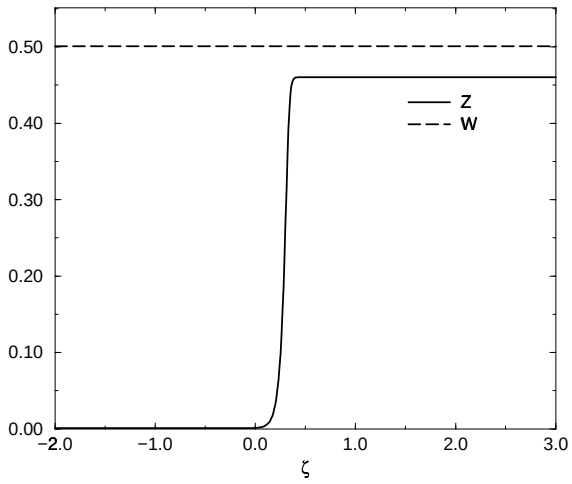

Figure 4: A1-L1$_0$ IPB for an $\langle hk0 \rangle$ orientation. Here $\delta^2 = 1.0$, $\epsilon^2 = {\lambda_z}^2 = 0.005$ and $T = T_c$.

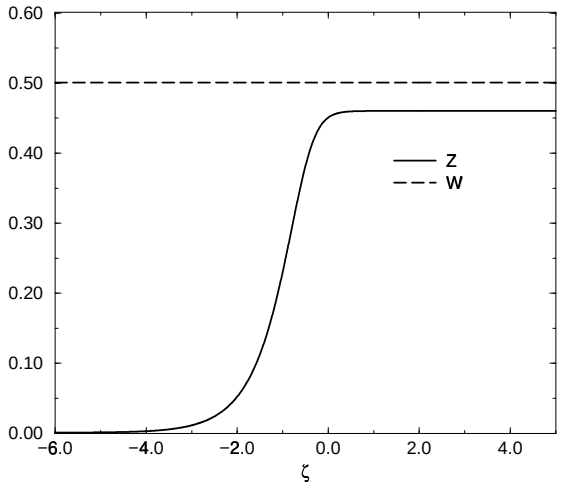

Figure 5: A1-L1$_0$ IPB for the [001] orientation. Here $T = T_c$, $\delta^2 = 1.0$, and ϵ^2 is arbitrary.

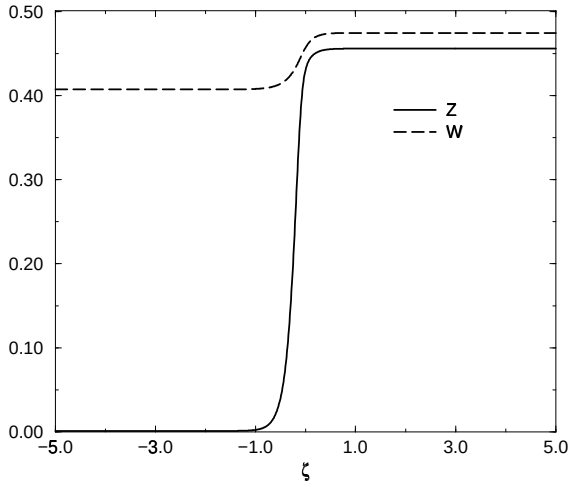

Figure 6: A1–L1$_0$ IPB for the [100] orientation. Here $\delta^2 = 1.0$, $\epsilon^2 = 0.005$ and $T = 2.5$.

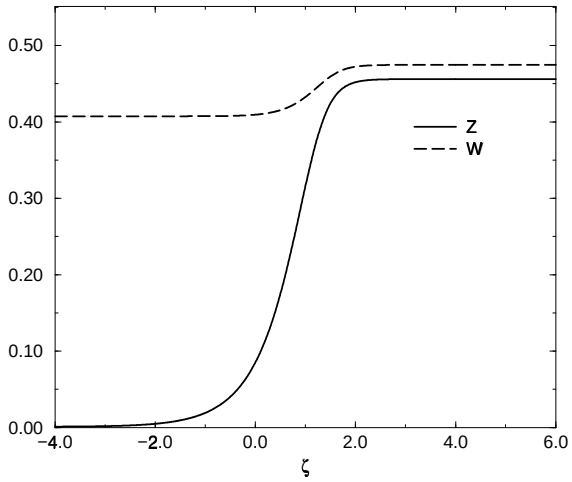

Figure 7: A1–$L1_0$ IPB for the [001] orientation. Here T= 2.5, $\delta^2 = 1.0$, and ϵ^2 is arbitrary.

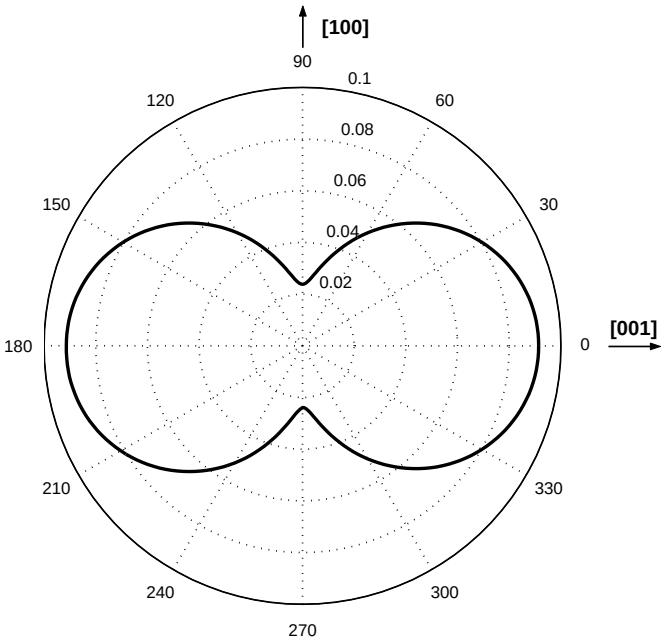

Figure 8: γ–plot for A1–$L1_0$ IPB for $\langle hk0 \rangle$. Here $T = 2.5$, $\delta^2 = 1.0$, $\epsilon^2 = 0.05$. Polar angle values are specified around the perimeter.

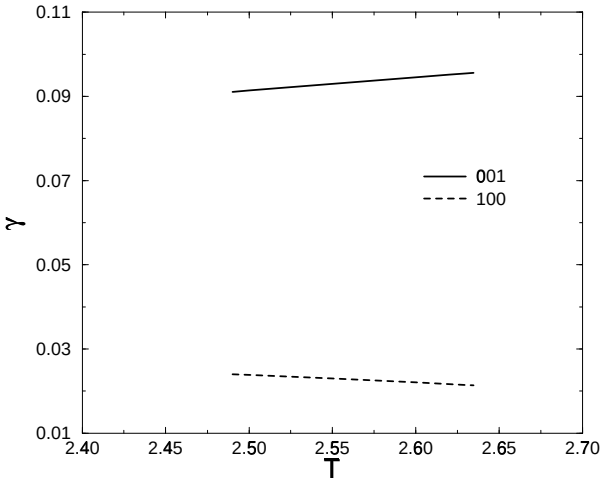

Figure 9: Variation of interfacial energy with temperature for [001] and [100] orientations for A1–L1$_0$ IPB. Here $\delta^2 = 1.0$, $\epsilon^2 = 0.05$.

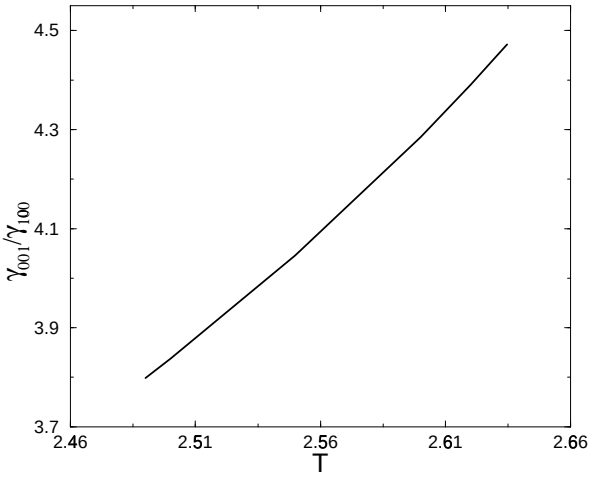

Figure 10: Level of anisotropy for A1–L1$_0$ IPB given by $\gamma_{001}/\gamma_{100}$ versus temperature. Here $\delta^2 = 1.0$, $\epsilon^2 = 0.05$.

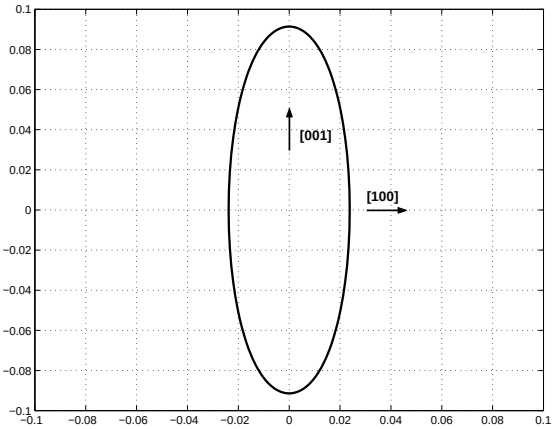

Figure 11: A cross section of the equilibrium shape for A1-L1$_0$ IPBs. Here, $T = 2.5$, $\delta^2 = 1.0$ and $\epsilon^2 = 0.05$.